https://doi.org/10.15360/1813-9779-2022-5-32-43



# Structural and Functional Reorganization of the Sensorimotor Cortex During Ligation of the Common Carotid Arteries (Experimental Study)

Lyubov M. Makarieva[1]*, Viktor A. Akulinin[1]*, Mikhail S. Korzhuk[1,2], Sergey S. Stepanov[1], Anastasia Y. Shoronova[1], Dmitry B. Avdeev[1], Irina G. Tsuskman[1]

[1] Omsk State Medical University, Ministry of Health of Russia, 12 Lenin Str., 644099 Omsk, Russia
[2] S.M. Kirov Military Medical Academy, 6 Academician Lebedev Str., B, 194044 St. Petersburg, Russia

# Структурно-функциональная реорганизация сенсомоторной коры при перевязке общих сонных артерий (экспериментальное исследование)

Л. М. Макарьева[1]*, В. А. Акулинин[1]*, М. С. Коржук[1,2], С. С. Степанов[1], А. Ю. Шоронова[1], Д. Б. Авдеев[1], И. Г. Цускман[1]

[1] Омский государственный медицинский университет Минздрава России, Россия, 644099, г. Омск, ул. Ленина, д. 12,
[2] Военно-медицинская академия им. С. М. Кирова, Россия, 194044, г. Санкт-Петербург, ул. Академика Лебедева, д. 6, литера «В»

**For citation:** *Lyubov M. Makarieva, Viktor A. Akulinin, Mikhail S. Korzhuk, Sergey S. Stepanov, Anastasia Y. Shoronova, Dmitry B. Avdeev, Irina G. Tsuskman.* Structural and Functional Reorganization of the Sensorimotor Cortex During Ligation of the Common Carotid Arteries (Experimental Study). *Obshchaya Reanimatologiya = General Reanimatology.* 2022; 18 (5): 32–43. https://doi.org/10.15360/1813-9779-2022-5-32-43 [In Russ. and Engl.]

## Summary

**Aim of the study.** To explore the structural and functional changes of neurons, glial cells, and synaptic terminals in layers I, III, and V of the sensorimotor cortex (SMC) of the rat brain after bilateral common carotid artery ligation (CCAL).

**Material and methods.** Incomplete cerebral ischemia was simulated by irreversible bilateral CCAL (2-vessel model of global ischemia without hypotension) on white rats ($n$=36). Comparative evaluation of the studied SMC structures was performed in the control group (intact rats, $n$=6) on days 1, 3, 7, 14, and 30 ($n$=30) after CCAL. Nissl, hematoxylin-eosin staining, and immunohistochemical reactions for NSE, MAP-2, p38, GFAP, and IBA1 were used. Numerical density of pyramidal neurons, astrocytes, oligodendrocytes, microglial cells, and relative area of p38-positive material (synaptic terminals) were determined. Statistical hypotheses were tested using nonparametric methods with Statistica 8.0 software.

**Results.** After CCAL, the number of degenerative neurons in rat brain SMCs increased. The peak of numerical density of unshrunken neurons was detected after day 1. Later, the numerical density of hyperchromic unshrunken neurons decreased, while that of shrunken neurons increased. These parameters did not reach the control values. The changes in SMC neurons were accompanied by an increase in the numerical density of microglial cells after day 1 and its subsequent decrease. Immunohistochemistry for IBA1 revealed signs of microglial cell activation such as change in shape and loss of processes. Maximum increase in the SMC density of oligodendrocytes was observed on day 7, and that of astrocytes on day 14 after CCAL. The maximum number of NSE-positive neurons occurred on day 1 after CCAL. There was a significant decrease in the number of NSE-positive neurons in SMC layer III on days 3, 7, and 14, and an increase in the number of NSE-positive neurons on day 30. The number of NSE-positive neurons in layer V of the SMC progressively decreased throughout the whole study period. The evolution of changes in the proportion of p38-positive material (synaptic terminal area) differed significantly between the layers of SMC. In the layers I and III, this parameter first decreased

**Correspondence to:**

Viktor A. Akulinin
E-mail: v_akulinin@outlook.com
Lyubov M. Makarieva
E-mail: lyuba.mamontova.07@gmail.com

**Адрес для корреспонденции:**

Виктор Александрович Акулинин
E-mail: v_akulinin@outlook.com
Любовь Михайловна Макарьева
E-mail: lyuba.mamontova.07@gmail.com

(days 1 and 3) and then increased (days 7, 14, and 30). In layer V of SMC, the activation of the protein expression was observed in the acute phase (days 1 and 3), then it decreased on days 7 and 14, and increased again on day 30. The changes found in the numerical density of neurons, glial cells and synaptic terminals were associated with dehydration and overhydration of SMC. We found strong to medium significant associations between the relative area of terminals and neuropil swelling and edema zones.

**Conclusion.** After CCAL, layers I, III, and V of the SMC of white rats revealed destructive and compensatory changes in neurons, glial cells, and inter-neuronal communication structures. Taken together, all these changes indicate a significant layer-by-layer variability of the neural tissue response to CCAL. Layer III (secondary projection complex) of the SMC was affected to a greater extent. Reorganization of neuronal-glial and interneuronal interrelations occurred along with a prominent neuropil overhydration.

***Keywords: ischemia; swelling and edema; neurons; synapses; sensorimotor cortex; immunohistochemistry; morphometrics***

**Conflict of interest.** The authors declare no conflict of interest.

Read the full-text English version at www.reanimatology.ru

## Introduction

The structural and functional organization of mammalian sensorimotor cortex (SMC) is well studied. Powerful bi- and polysynaptic connections between its layers and modules have been described in the literature [1–4].

The structure and functions of neurons, glial cells and inter-neuronal communication systems (dendrites, synapses) of SMC can be altered as a result of ischemia. These changes lead to reorganization of inter-neuronal and neuroglial interactions [5–7]. We have previously shown that irreversible bilateral ligation of common carotid arteries (LCCA) caused an increase in the numerical density of abnormal neuronal forms (hypochromic, hyperchromic shrunken/non-shrunken neurons, ghost cells) and appearance of neurons with pericellular edema in SMC starting from day 1 after LCCA. However, neuronal response and neuroglial interaction were not identical in different layers. Thus, in layer III of SMC, the numerical density of irreversibly altered neurons (hyperchromic shrunken) progressively increased and reached its maximum values 30 days after LCCA, while in layer V of SMC the number of irreversibly altered neurons decreased after 14 and 30 days compared to the previous time intervals [8, 9].

Ischemic damage of the brain neurons entails severe neurological consequences. Therefore, special attention has been focused on the studies of cerebrovascular diseases, which are the main cause of mortality worldwide [10–12]. Comprehensive morphological and morphometric studies of neurons, glial cells and inter-neuronal communication structures are required for a more detailed insight into the neural tissue response to ischemia and defense mechanisms ensuring neuronal survival in ischemia. Therefore, the aim of our study was to compare the histological and immunohistochemical data characteristic of structural and functional changes in neurons, glial cells and synaptic terminals in layers I, III and V of rat brain SMCs after bilateral LCCA. Special emphasis was placed on determining the role of overhydration of neuropil where the synapses, neuronal and astrocytic processes are localized.

## Material and Methods

The study was carried out at Omsk State Medical University (approved by the University Ethics Committee, protocol 123, October 9, 2020). White Wistar rats weighing 250–300 g were used as experimental animals. Studies were conducted in accordance with the guidelines of the International Committee on laboratory animals supported by WHO, the European Parliament Directive 2010/63/EU of 22.09.2010 «On protection of animals used for scientific purposes».

The experiment was performed on sexually mature male Wistar rats ($n$=36). After premedication (atropine sulfate 0.1 mg/kg, subcutaneously), the animals were injected with Zoletil 100 (10 mg/kg, intramuscularly). Incomplete global cerebral ischemia was simulated by irreversible bilateral LCCA (2-vessel model of subtotal ischemia, without hypotension). Intact rats ($n$=6) served as a control. The animals were withdrawn from the experiment 1, 3, 7, 14, and 30 days after LCCA ($n$=30) under anesthesia (Zoletil 100). The cerebral vasculature was flushed by injecting 100–125 ml of 0.9% NaCl solution and Fragmin (5000 units) into the left ventricle of the heart and fixated by perfusion with 30 ml of 4% paraformaldehyde solution in phosphate buffer (pH 7.2–7.4) through the aorta at 90–100 mm Hg for 15 min. The brains were placed in 4% paraformaldehyde solution and stored in the refrigerator at + 4°C. One day later, the obtained material was embedded in homogenized paraffin (HISTOMIX®) using an STP 120 machine. Serial frontal sections (4 μm thick) were prepared using an HM 450 microtome (Thermo) at the SMC level, that is 1.2 to (–3.0) mm from bregma [13].

General qualitative evaluation of neural tissue and determination of the numerical density of neurons (only neurons with visible nuclei were counted) and glial cells were performed on preparations stained with thionine according to the Nissl method. Neuron identification was performed by the histochemical reaction for neuron specific enolase (NSE) using rabbit polyclonal antibodies at 1:100 dilution (PA5-27452), to identify glial fibrillary acidic protein (GFAP) of astrocytes for astrocyte identification and cytoskeleton studies (MA5-12023), the murine IgG1

monoclonal antibodies (clone ASTRO6) were used. The antibodies to IBA1 for identification of microglia by the calcium-binding protein specific for microglia (PA5-21274) were detected using tje rabbit polyclonal antibodies, 1: 100 dilution (all the above manufactured by ThermoFisher, USA). The neuronal cytoskeleton was studied using the immunohistochemical reaction for MAP2 (microtubule-associated protein 2, ab32454), rabbit polyclonal antibody, 1 μg/ml dilution (Abcam, USA). Synaptic terminals were studied using synaptophysin (p38) (PA0299) using the murine monoclonal antibody, clone 27G12, ready-to-use (Bond Ready-to-Use Primary Antibody; Leica Biosystems Newcastle Ltd, UK).

After reaction with primary antibodies, the sections were incubated with appropriate secondary antibodies, DAB (3,3'-diaminobenzidine) chromogen, stained with hematoxylin, and embedded in polystyrene. A NovolinkTM (DAB) Polymer Detection System (Leica Biosystems Newcastle Ltd, United Kingdom) multimeric kit was used for imaging. The preparations were made in accordance with the instructions of the reagent manufacturer.

Images were taken using a Leica DM 1000 microscope (GXCAM-DM800 Unique Wrap-Around 8MP AUTOFOCUS USB, pixel size 1.4×1.4 μm) and saved as tiff files (2592×1944 pixels) with subsequent upscaling using Photoshop CC (to 3780×2835 pixels/cm, 600 pixels/inch resolution).

In order to achieve maximum contrast and sharpness of the image, image adjustment was performed using a Camera Raw filter (contrast, white balance, and sharpness) in Photoshop CC. Morphometric examination was performed using ImageJ 1.53 software.

Enhance Contrast filter (https://imagej.nih.gov/ij/docs/menus/process) with subsequent image processing in Threshold (selection of synaptophysin labels and edema areas) was used to detect p38-positive terminals and edema and swelling zones in neuropil. Selection was performed for each ROI (20×20 μm) manually (Over/Under). Later, histograms of pixel distribution by brightness were plotted, and the obtained results (List) were transferred to Excel for further processing. Twenty ROIs were selected per time point using a random number generator.

Statistical hypotheses were tested using nonparametric criteria such as paired comparison (Mann–Whitney *U*-test, Wilcoxon test), analysis of variance (ANOVA Kruskal–Wallis, Friedman test),

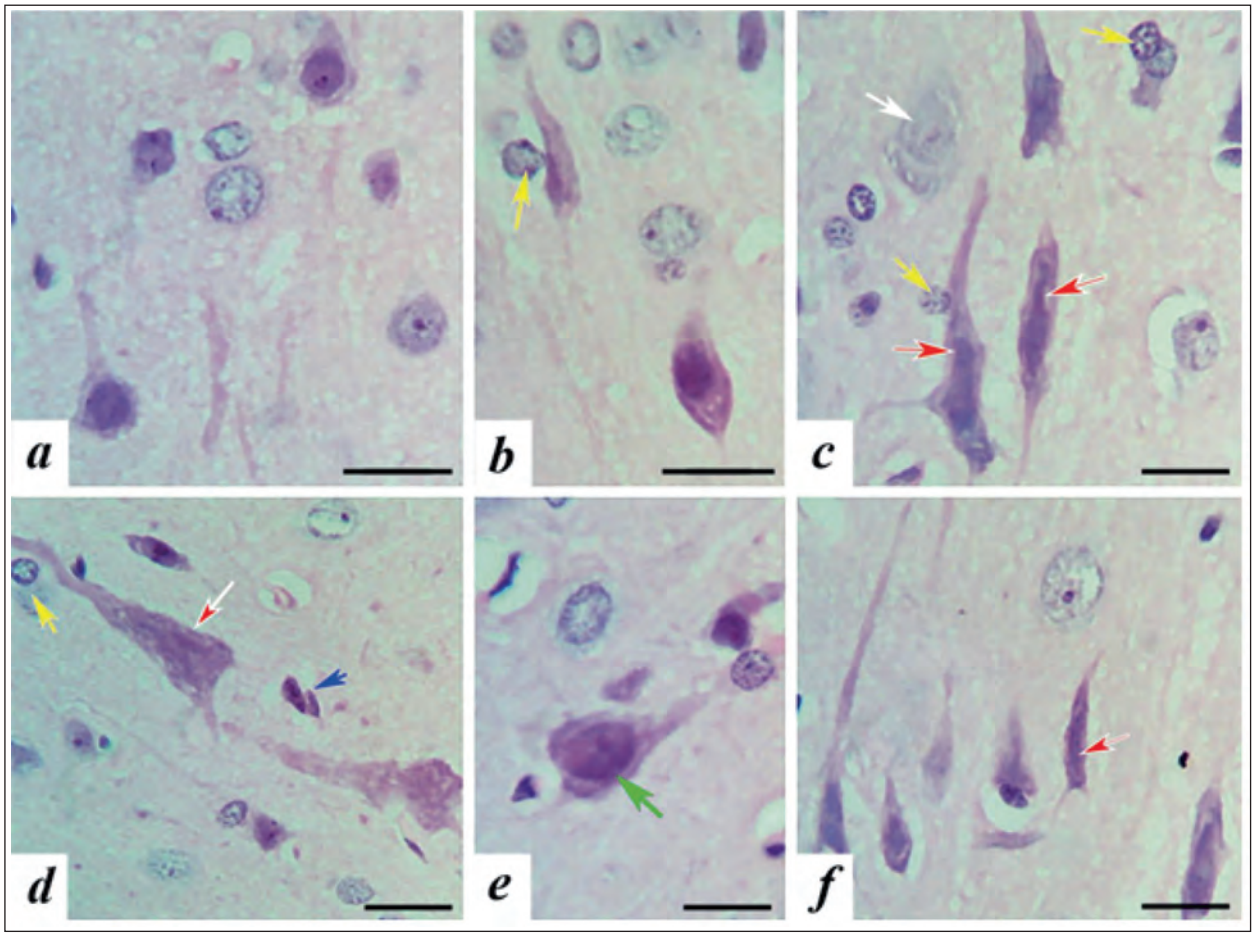


**Fig. 1. Pyramidal neurons of layers III (*a, b*) and V (*c–f*) SMC at different stages of destruction after LCCA.**
**Note.** Hyperchromic non-shrunken neurons (green arrows); shrunken neurons (red bars); ghost cells (white arrows); gliocytes (yellow arrows); microgliocytes (blue arrows). Hematoxylin-eosin staining, magnification ×100, scale 20 μm.

paired correlation analysis (Spearman method). Multiple regression analysis was used to assess the influence of the compared variables on each other. Independence of the observations was tested using the Durbin–Watson criterion. Statistica 8.0 software package (StatSoft, USA) was used. Quantitative data in the study were presented as medians (Me — 50% quartile, Q2), interquartile ranges (Q1–Q3 — 25–75% quartiles), (Min–Max), percentages (%) [14].

## Results and Discussion

Previously, we found that normochromic neurons predominated in layers III and V of SMCs of control animals. There were no signs of hydropic degeneration (vacuolization of nuclei and cytoplasm, edema and swelling), necrosis (colliquative and coagulative) and reactive gliosis [8, 9].

After LCCA, layers III and V of SMC showed *in vivo* reversible and irreversible changes in neurons corresponding to different stages of degeneration. These changes were observed in the cytoplasm and nucleus of pyramidal neurons (vacuolation, homogenization of cytoplasm, changes in perikaryon and nuclear shape, hypo- and hyperchromia of nuclei and cytoplasm, karyolysis) and were accompanied by edema and swelling. Reversibly damaged neurons did not demonstrate any gross destruction of nucleus and cytoplasm, their nuclei were preserved, but had altered staining properties (hyperchromic non-shrunken neurons). Pyramidal neurons with reversible changes were found in layers III and V of the SMC during the entire study period (Fig. 1, *a–f*).

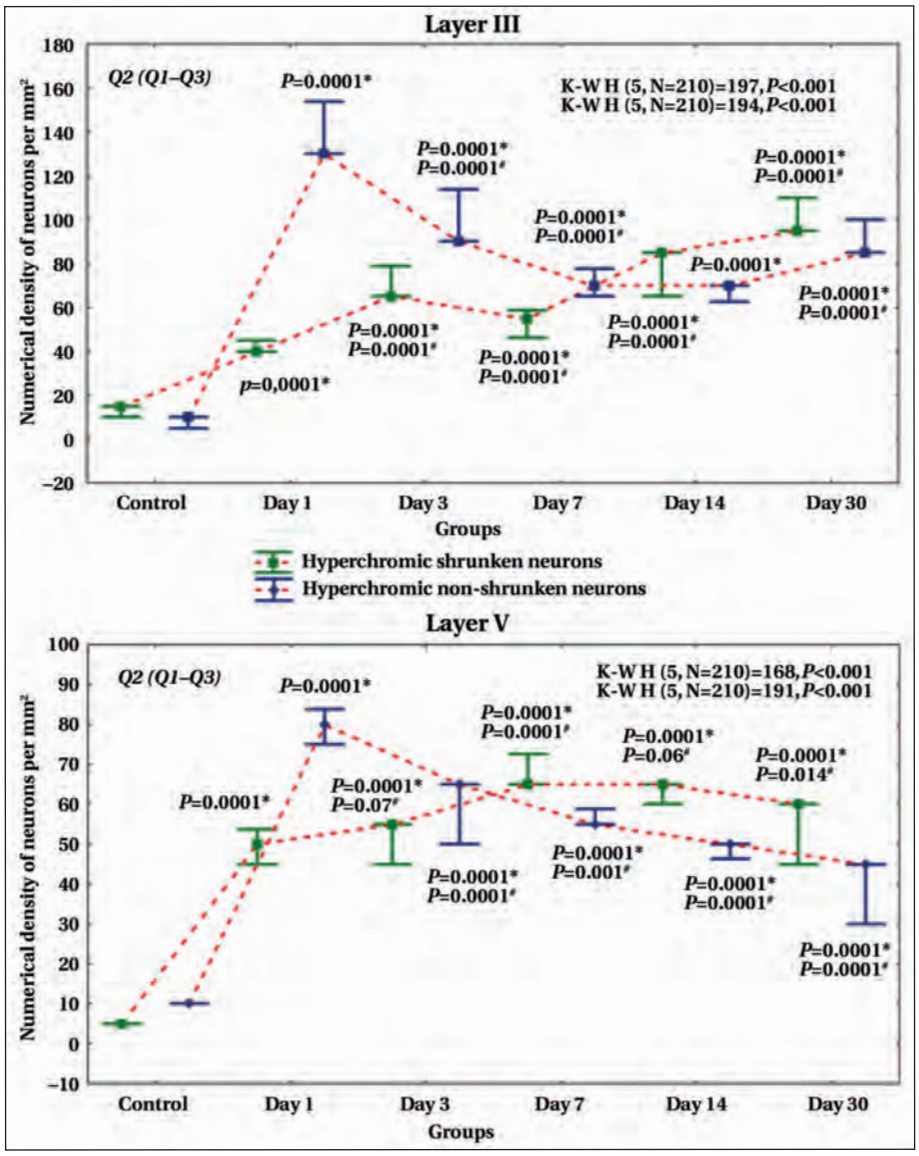


**Fig. 2. Numerical density of hyperchromic non-shrunken and shrunken neurons in layers III and V SMC in the control, 1, 3, 7, 14 and 30 days after LCCA.**

**Note.** * — vs the control; # — vs the previous time point (Mann–Whitney *U*-test). Differences were considered significant at $P<0.05$. Data presented as medians (Q2) and 25–75% quartiles (Q1–Q3). Differences between all time points after LCCA are significant based on the ANOVA Kruskal–Wallis test (K–W).

The numerical density of hyperchromic non-shrunken neurons in layer III SMC was not the same at different study periods, reaching its maximum values 1 day after LCCA, and a significant decrease in the numerical density of hyperchromic non-shrunken neurons in layer III SMC was noted on days 3–14, followed by a significant increase on day 30 vs the previous day (Fig. 2, *a*). In layer V of the SMC, the numerical density of hyperchromic non-shrunken neurons peaked 1 day after LCCA and significantly decreased by day 30 of the study, reaching the lowest values for the entire study period (Fig. 2, *b*).

Irreversible *in vivo* degeneration of neurons manifested as intense eosinophilia of the nucleus and cytoplasm, karyopyknosis, loss of nuclear boundaries, cytoplasm homogenization and reduction of the nucleus and perikaryon size (hyperchromic shrunken neurons and ghost cells) when stained with hematoxylin-

eosin (Fig. 1). The numerical density of hyperchromic shrunken neurons in layer III of the SMC was higher than the control values throughout the study period. In the acute period of ischemia (days 1 and 3), their significant increase in layer III of SMC was seen as compared to controls, on day 7, their density decreased (by 15.4% as compared with day 3), and on days 14 and 30, their density increased vs day 7, with a peak on day 30 after LCCA (Fig. 2, *a*). The maximum increase in the number of shrunken neurons in layer V of the SMC was observed on day 7 after LCCA. On days 14 and 30, there was a significant decrease in the number of shrunken neurons as compared to the previous day (Fig. 2, *b*).

After LCCA, the reorganization of glial cells was observed, manifesting as a change in their numerical density and neuroglial ratio. Thus, the maximum numerical density of microglial cells in layers III and V of SMC was observed after day 1, that of astrocytes after day 14, and that of oligodendrocytes after days 7 and 14 (layer III) and 7 (layer V) (Fig. 3).

After days 1 and 3, activation of microglial cells probably occurred, which manifested as a changing the shape of the cells to round or oval and loss of the processes. These changes were detected in IBA1-positive material (Fig. 4 *c, d*). Similar causal relationships have been noted in the literature. Thus, as a result of activation, a change in the shape of microglial cells to oval with the loss of processes was suggested to facilitate the movement of glial cells [15–17]. These changes are necessary for nerve tissue repair after ischemic damage. An increase in the numerical density of oligodendrocytes was observed. The maximum numerical density of these cells was detected 7 and 14 days after LCCA (Fig. 3).

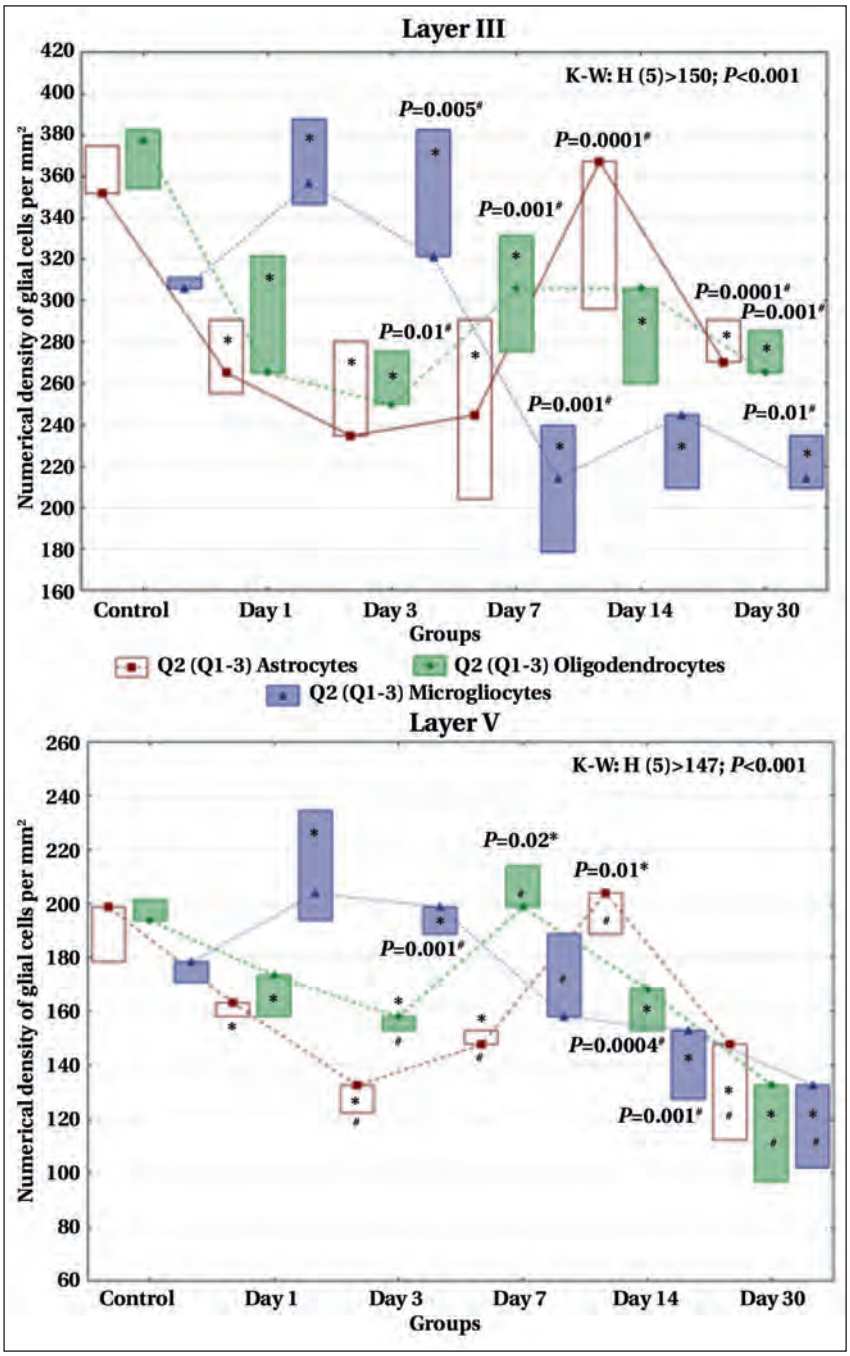


**Fig. 3. Numerical density of astrocytes, oligodendrocytes and microgliocytes of layer III and V SMC in the control group and after irreversible bilateral LCCA on days 1, 3, 7, 14, and 30.**

**Note.** * — pairwise comparison vs the controls; # — vs the previous time point (Mann–Whitney *U*-test). Separate asterisk and tick indicate *P*=0.0001. Data presented as medians (Q2) and 25–75% quartiles (Q1–3). Differences between all the time points after LCCA were significant based on the ANOVA Kruskal–Wallis (K–W) test. The differences were considered significant at *P*<0.05.

The peak of astrocyte numerical density was observed 14 days after LCCA in layers III and V of the SMC. Starting 1 day after LCCA, hypertrophy of astrocyte processes was observed (Fig. 4, *a, b*). Astrocytes are known to be involved in the regulation of extracellular levels of glutamate, gamma-aminobutyric acid, adenosine and synaptic plasticity [18, 19].

According to the literature, astrocyte hypertrophy results from their response to impaired ion homeostasis and energy balance after LCCA. In re-

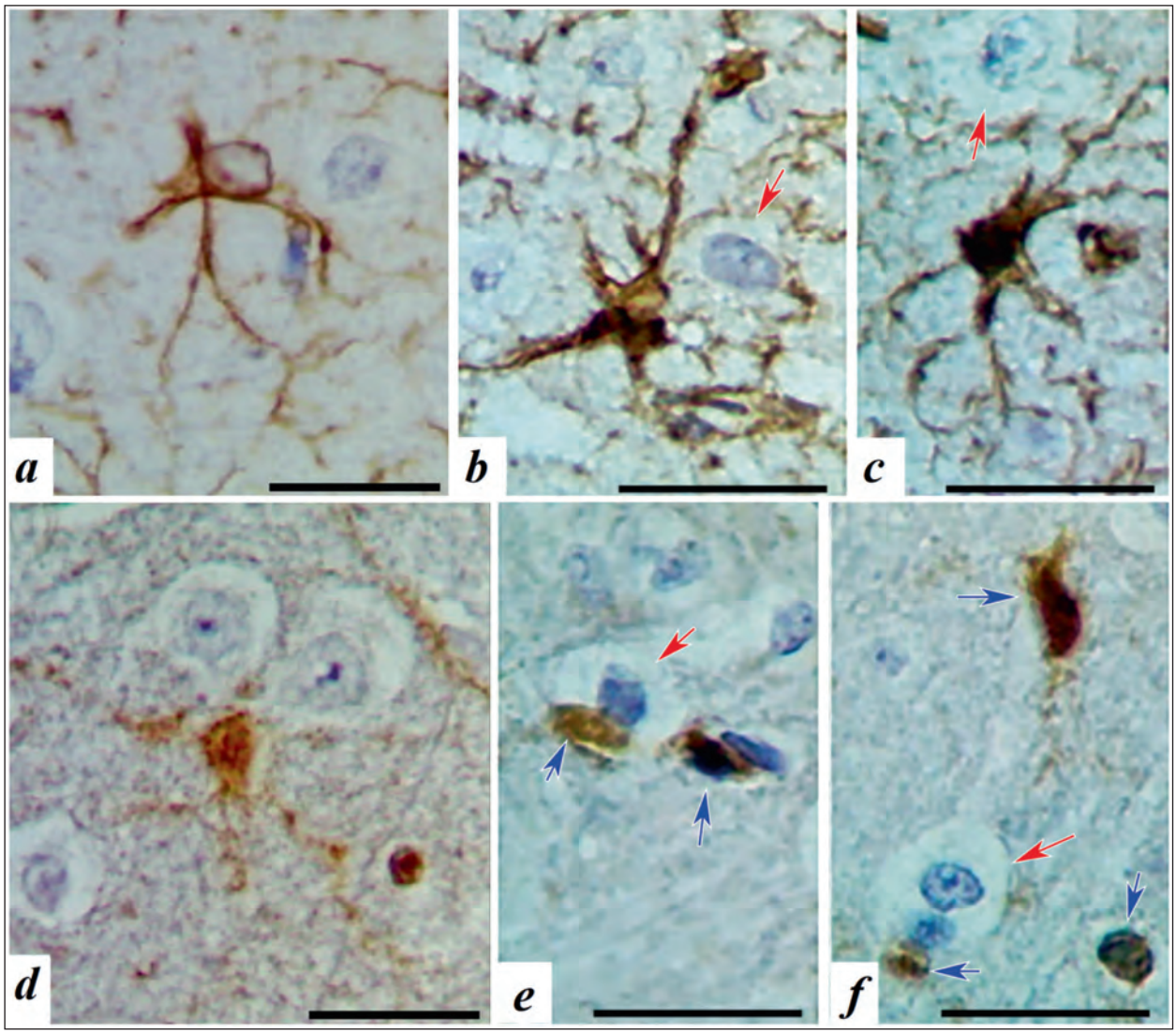


**Fig. 4. Astrocytes (*a, b, c*) and microgliocytes (*d, e, f*) of layer III SMC in the control group (*a, d*) and on day 1 after LCCA (*b, c, e, f*).**
**Note.** Astrocytes around pyramidal neurons (red arrow); process hypertrophy; elongated shape of microgliocyte bodies (blue arrow). Staining: GFAP reaction (*a, b*), IBA1 reaction (*c, d*). Magnification ×100; scale 20 μm.

sponse to ischemic damage, astrocytes try to stabilize the balance of substances and fluid in the intercellular space [20]. The activation of all glial cells as components of a single integrated cellular reparation system of the brain has been suggested. Probably, it is necessary for protection and repair of the nervous tissue after ischemic damage following irreversible bilateral LCCA and can promote activation of undamaged neurons and functional replacement of the dead neurons [21–23].

According to the morphometric study of NSE-positive material in layers III and V of the SMC, the maximum increase in the proportion of NSE-positive neurons was observed in the acute phase of ischemia (after day 1). A significant progressive decrease in the proportion of NSE-positive neurons was detected in layer III of the SMC on days 3–14 after LCCA as compared to day 1, and an increase was recorded after day 30 as compared to the previous day (Fig. 5).

These changes were associated with the significant increase in the numerical density of hyperchromic non-shrunken neurons (Fig. 2), which probably indicates an increase in NSE expression in neurons 30 days after LCCA [24, 25]. The proportion of NSE-positive neurons in layer V of the SMC throughout the study period (1, 3, 7, 14 and 30 days after LCCA) was significantly higher than in the controls (Fig. 5).

Immunohistochemical studies (p38) have shown that synaptic terminals in all SMC layers were distributed in the neuropil (axodendritic), perikaryons (axosomal), and large dendrites (axodendritic and axospinous synapses) of pyramidal neurons (Fig. 6, *a–c*). At the same time, different densities of this synaptic protein were visually observed in the layers of control animals and after LCCA. The differences in the layers were related to the specifics of their organization with the prevalence of neuropil and

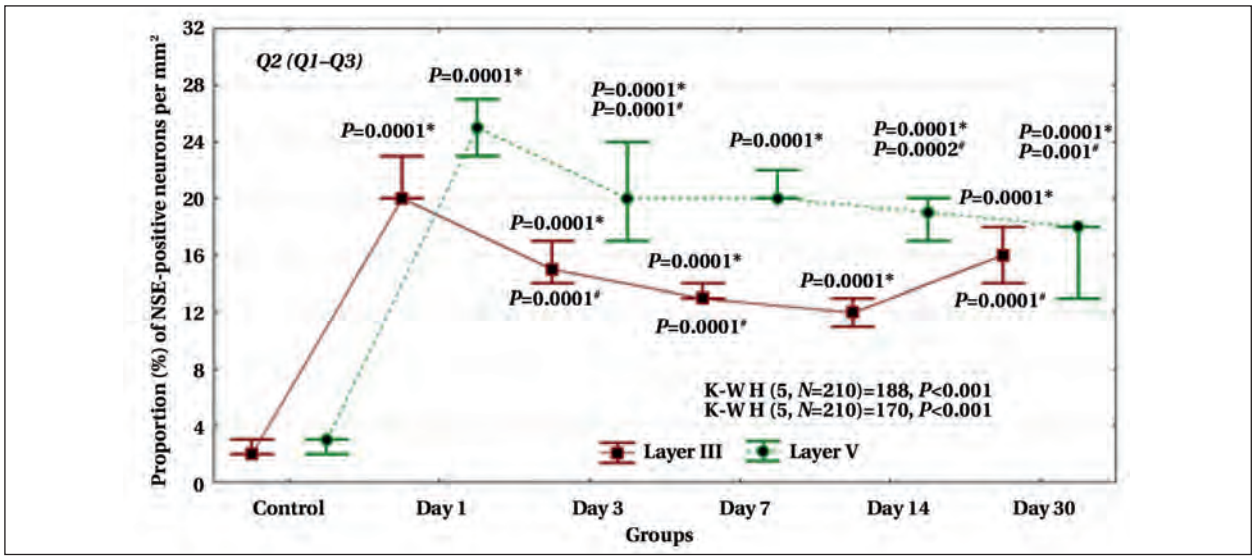


**Fig. 5. Proportion (%) of NSE-positive neurons in layers III and V SMC in the control group and after LCCA.**
**Note.** * — pairwise comparison with the control; # — vs the previous time point (Mann–Whitney *U*-test). Separate asterisk and tick indicate *P*=0.0001. Data presented as medians (Q2) and 25–75% quartiles (Q1–3). Differences between the time-points after LCCA were significant based on the ANOVA Kruskal–Wallis (K–W) test. The differences were considered significant at *P*<0.05.

apical dendrites of the underlying pyramidal neurons in the molecular layer. Small and large edema and swelling foci in the compared layers could also be visually identified. They appeared as areas of maximum image brightness (Fig. 7, *a–e*; Fig. 8, *a–e*).

Using the analysis of pixel distribution histograms of neuropil images (zones of interest of 400 μm²) we identified the relative area of terminals and edema and swelling zones. The main steps of this approach are shown in the Fig. 9.

Significant changes in the studied morphometric independent variables vs the control and over the follow-up period (days 1–30) were revealed (see Table). Peaks of increase in the relative area of terminals and edema and swelling zones were observed, as well as correlations between them.

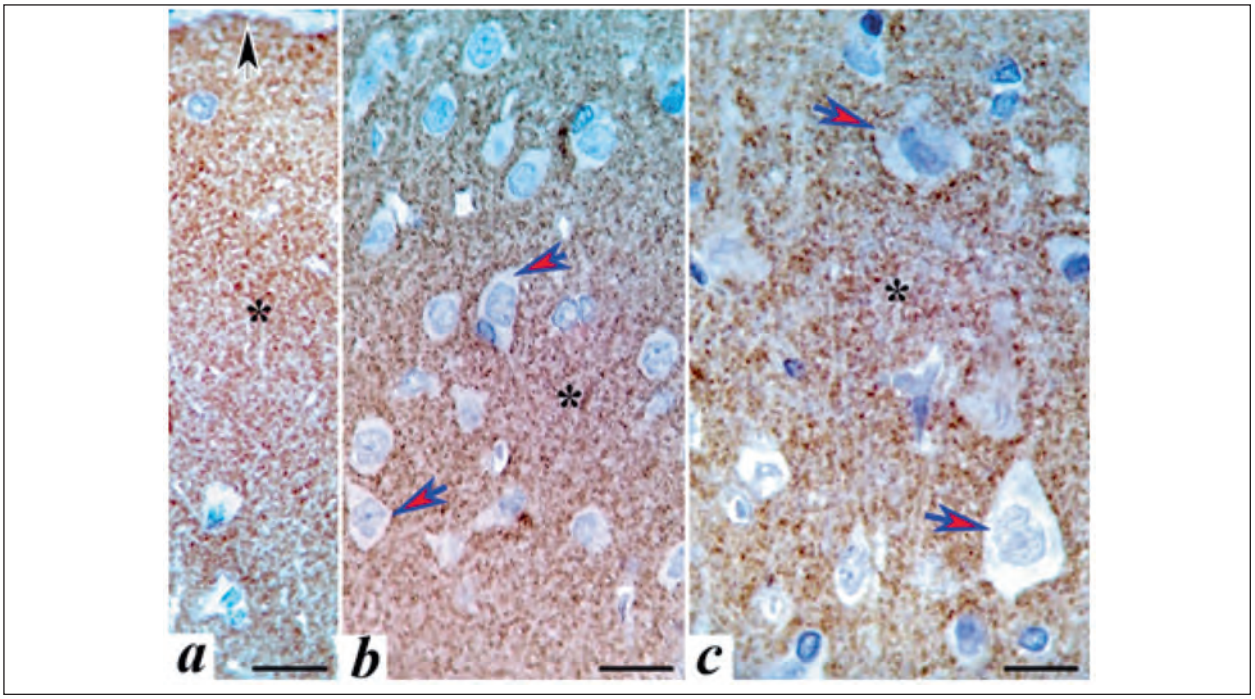


**Fig. 6. Neuropil (*) and neurons (red arrows) of layers I (*a*), III (*b*) and V (*c*) SMC of rats after staining for a specific neuronal protein of synaptic terminals (synaptophysin, brown granules).**
**Note.** *a, b* — control; *c* — day 1 after LCCA. Black arrow indicates the outer (pial) surface of layer I. Immunohistochemical staining for synaptophysin, hematoxylin counterstaining. Magnification ×100, scale 20 μm.

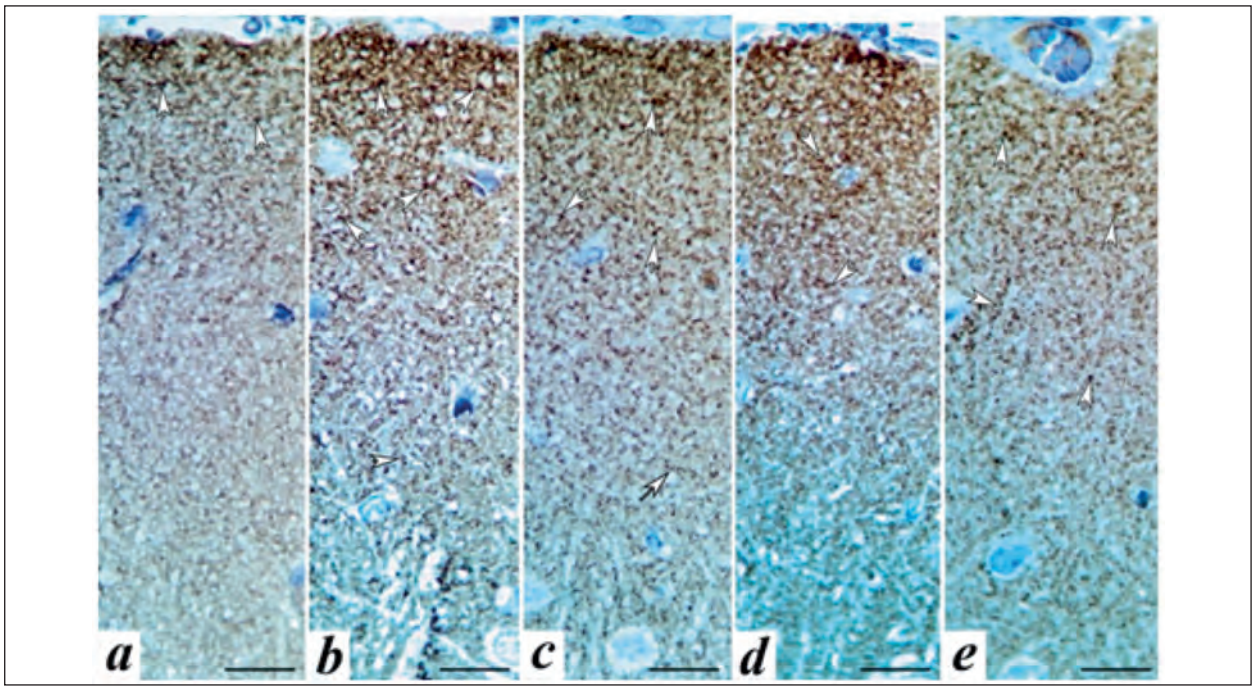


**Fig. 7. Neuropil of layer III of SMC in rats on days 1 (*a*), 3 (*b*), 7 (*c*), 14 (*d*), and 30 (*e*) after LCCA.**
**Note.** Different density of p38-positive terminals (arrows) and small vacuoles (light rounded). Immunohistochemical reaction for synaptophysin, hematoxylin counterstaining. Magnification ×100, scale 20 μm.

Using Friedman's ANOVA (multiple comparisons of the related variable), we found significant differences in the relative area of p38-positive material (synaptic terminal area) in the compared SMC layers (df=2) in all groups. The maximal differences were noted in the acute phase, when the highest values of the $\chi^2$ criterion and the lowest p-values were observed. Thus, $\chi^2$ was 6.9 ($P$=0.03) in the controls, 15.2 ($P$=0.001) on day 1, 5.2 ($P$=0.001) on day 3, 11.4 ($P$=0.003) on day 7, 12.8 ($P$=0.002) on day 14, and 10.9 ($P$=0.004) on day 30.

Analysis of the relative area of neuropil edema and swelling of the compared layers also showed greater differences in this variable in the acute

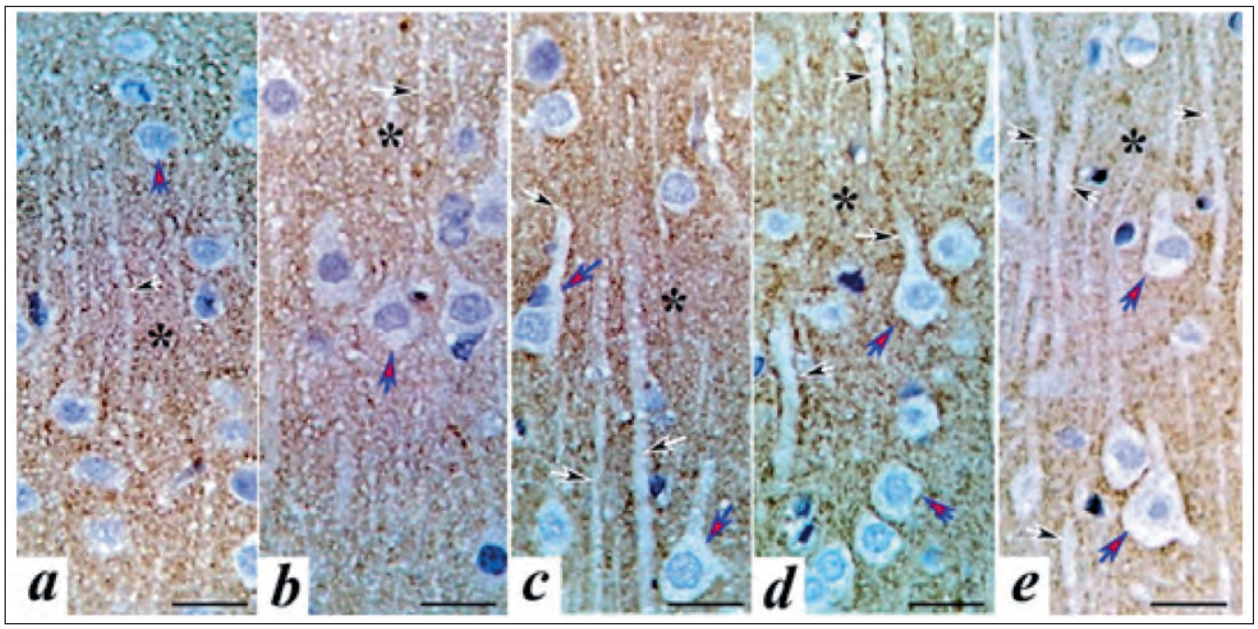


**Fig. 8. Neurons (red arrows), dendrites (black arrows), and neuropil (*) of layer III of rat SMC on days 1 (*a*), 3 (*b*), 7 (*c*), 14 (*d*), and 30 (*e*) after LCCA.**
**Note.** Different density of p38-positive terminals (brown particles) and small vacuoles (light rounded) is shown. Immunohistochemical staining for synaptophysin, hematoxylin counterstaining. Magnification ×100, scale 20 μm.

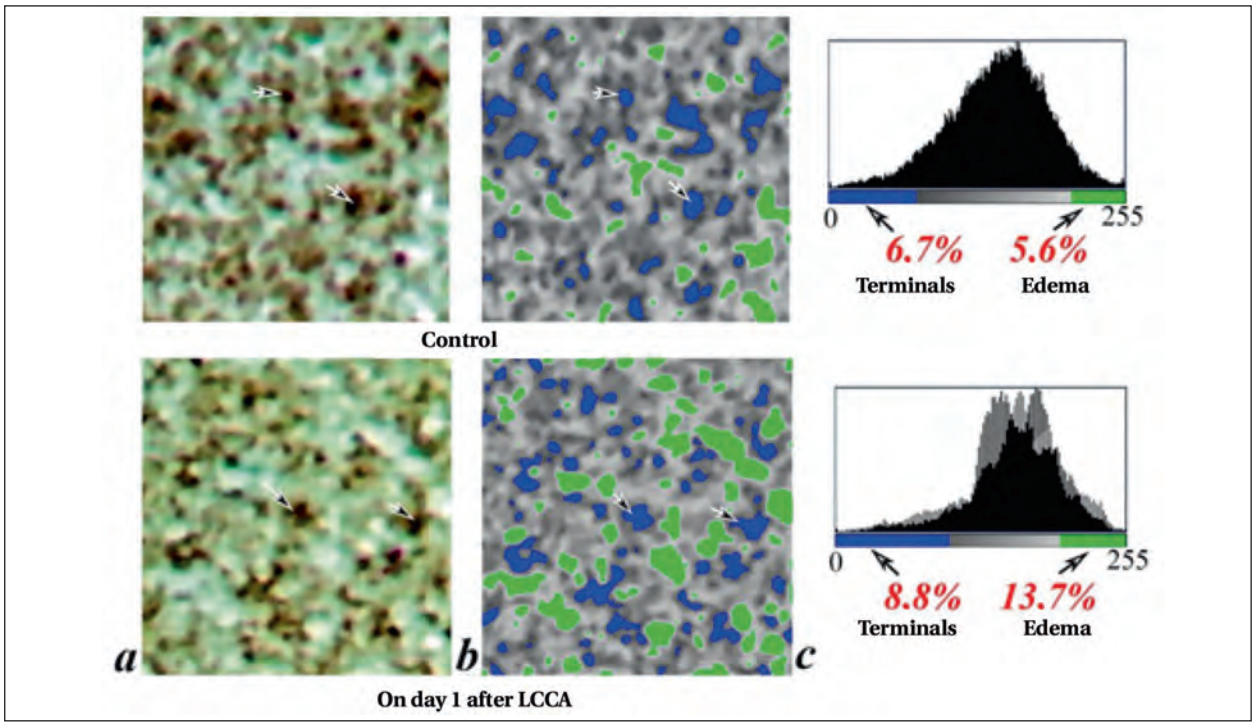


**Fig. 9. Main stages of assessment of the relative area of terminals and small foci of edema (%) in the neuropil of layer I of rat SMC using the ImageJ 1.53 software.**

**Note.** *a* — initial ROI (400 μm², RGB, Enhance Contrast filter); *b* — after image processing in Threshold (selection of synaptophysin labels and edema foci); c — distribution histogram of ROI image pixels with indication of their number and brightness. Arrows pointing at ROI indicate terminals at different stages of analysis. Terminals are stained blue, foci of edema, green. Immunohistochemical reaction for synaptophysin, hematoxylin counterstaining. Magnification ×100, scale on the ROI side 20.0 μm (area, 400 μm²).

phase of disease: $\chi^2$ was 2.1 ($P$=0.4) in the control group, 20.0 ($P$=0.0001) on day 1, 18.2 ($P$=0.0001) on day 3, 13.4 ($P$=0.001) on day 7, 15.8 ($P$=0.0004) on day 14, 2.7 ($P$=0.26) on day 30. A paired comparison allowed us to reject the null hypothesis for these variables (Table 1, Wilcoxon test). In the neuropil of the studied layers 30 days after LCCA, there could be a partial restoration of water and ionic balance of SMC cells.

According to paired Spearman correlation analysis of the entire observation period (1–30 days), a strong and weak negative relationship ($r$=–0.52, $P$=0.0000 and $r$= –0.47, $P$=0.004, respectively) was found between the independent variables (relative area of terminals and neuropil edema and swelling areas) in layers I and III of SMC. A moderate positive relationship was seen in the layer V of SMC ($r$=0.54, $P$=0.0004). This could be due to the relation between the SMC layer and changes in terminal area and edema and swelling zones after LCCA. In the control values (for all layers), no significant relationships between these variables were found.

Importantly, a moderate positive correlation ($r$=0.58, $P$=0.02) on day 1 after LCCA and a negative correlation at other timepoints ($r$=–0.59, $P$=0.02 on day 3, $r$= –0.56, $P$=0.02 on day 7, $r$=–0.64, $P$=0.04 on day 14, and $r$=–0.50, $P$=0.04 on day 30) was found in layer I of SMC. For layer III of SMC, significant temporal correlations were found only after day 3 ($r$=–0.94, $P$=0.005), but their character was identical to that of layer I of SMC. This probably indicated a change in the causal relationships in these layers after day 3 or the new discriminative factors, such as compensatory increase in the new synaptic vesicles and terminals and hypertrophy of astrocyte processes. The layer V of SMC was characterized by a strong negative ($r$=–0.90, $P$=0.0003) correlation after day 3 and moderate negative correlation ($r$=–0.68, $P$=0.03) after day 7. Thus, we can assume that days 3 and 7 after LCCA were a certain breakpoint when the change in the domination of damage and recovery processes occurred. These changes followed a specific pattern depending on layer, which was confirmed by the character and strength of correlation during specific time periods.

The multiple regression analysis showed that on day 3 after LCCA (period of maximum strength relationship between the variables), a 1% change in the area of edema and swelling zones resulted in the following changes in terminal area: 0.57% in layer I of SMC, 0.31% in layer III of SMC, and 0.72% in layer V SMC. The coefficient of determination of regression models was 34% ($P$=0.02), 72% ($P$=0.03) and 80% ($P$=0.01), respectively. The Durbin-Watson criterion was 1.5–2.0 (acceptable range from 1 to 3), which indicated the reliability of the results.

**Relative areas of p38-positive synaptic terminals and small foci of edema and swelling of the neuropil of various layers of rat SMC in normal animals and after LCCA, *Q2* (*Q1–Q3*).**

| Groups | The sensorimotor cortical levels and parameter values | | | | | |
|---|---|---|---|---|---|---|
| | Layer I | | Layer III | | Layer V | |
| | RAT | RAES | RAT | RAES | RAT | RAES |
| Control | 12.8 (10.8–15.2) | 9.6 (7.9–10.7) | 7.95 (7.6–8.4) *P*=0.02$^{I–III}$ | 8.8 (7.1–9.7) | 7.9 (7.4–8.2) *P*=0.01$^{I–V}$ | 7.2 (6.9–8.5) *P*=0.02$^{I–V}$ |
| Day 1 | 11.4 (8.8–14.3) | 17.3 (15.1–19.6) *P*=0.0001* | 5.2 (4.7–7.2) *P*=0.001* *p*=0.001$^{I–III}$ | 29.7 (27.9–31.7) *P*=0.0000* *P*=0.005$^{I–III}$ | 12.0 (11.0–13.0) *P*=0.0003* *P*=0.005$^{III–V}$ | 14.5 (10.6–16.4) *P*=0.0004* *P*=0.005$^{I–V}$ *P*=0.005$^{III–V}$ |
| Day 3 | 9.2 (7.0–11.7) *P*=0.04* | 20.2 (14.5–21.3) *P*=0.0001* | 4.0 (2.8–4.5) *P*=0.0001* *P*=0.01** *P*=0.001$^{I–III}$ | 23.7 (22.5–28.9) *P*=0.0001* *P*=0.019** | 13.5 (11.8–14.6) *P*=0.0002* *P*=0.005$^{III–V}$ | 12.8 (11.5–15.2) *P*=0.0002* *P*=0.01$^{I–V}$ *P*=0.005$^{III–V}$ |
| Day 7 | 15.1 (9.2–18.9) *P*=0.03** | 12.8 (10.5–17.0) *P*=0.007* *P*=0.006** | 6.7 (5.7–6.9) *P*=0.02* *P*=0.0004** *P*=0.002$^{I–III}$ | 16.9 (13.7–18.6) *P*=0.0001* *P*=0.001** *P*=0.02$^{I–III}$ | 9.8 (9.0–10.1) *P*=0.02* *P*=0.001** *P*=0.01$^{I–V}$ *P*=0.03$^{III–V}$ | 8.2 (7.7–8.9) *P*=0.03* *P*=0.001** *P*=0.005$^{III–V}$ |
| Day 14 | 18.9 (13.4–23.4) *P*=0.01* | 9.8 (8.4–10.6) *P*=0.01** | 5.5 (4.4–9.8) *P*=0.001$^{I–III}$ | 21.0 (18.5–23.4) *P*=0.0001* *P*=0.005** *P*=0.005$^{I–III}$ | 9.8 (8.5–10.6) *P*=0.01* *P*=0.04$^{I–V}$ *P*=0.04$^{III–V}$ | 11.2 (7.8–12.1) *P*=0.001* *P*=0.005$^{III–V}$ |
| Day 30 | 16.2 (12.5–24.0) | 9.7 (8.1–14.1) | 8.4 (7.2–10.6) *P*=0.049** *P*=0.007$^{I–III}$ | 15.0 (11.5–18.4) *P*=0.0001* *P*=0.01** | 12.4 (12.3–12.8) *P*=0.0002* *P*=0.001** *P*=0.01$^{III–V}$ | 10.1 (8.9–11.2) *P*=0.001* |
| ANOVA K–W | H(4)=18.6 *P*=0.001$^{\#}$ | H(4)=36.3 *P*=0.0000$^{\#}$ | H(4)=27.4 *P*=0.0000$^{\#}$ | H(4)=32.5 *P*=0.0000$^{\#}$ | H(4)=15.9 *P*=0.003$^{\#}$ | H(4)=13.3 *P*=0.01$^{\#}$ |

**Note.** * — significant differences vs the control at $P<0.05$; $^{\#}$ — significant differences vs the previous time point (Mann–Whitney *U*-test). $^{I–III}$, $^{I–V}$, $^{III–V}$ —comparison between the corresponding layers (Wilcoxon test) at $P\leqslant 0.02$. $^{\#}$ — differences between time points after LCCA were significant based on the one-way multiple analysis (ANOVA Kruskal–Wallis) test. RAT, relative area of the terminals, RAES, relative area of the edema and swelling zones. The data are presented as medians and interquartile ranges.

Thus, on day 3, only 34% of the relative area of neuropil edema and swelling zones could be explained by the lucid-type (edematous) type of terminal destruction in the layer I of SMC, while 66% were probably caused by hydropic degeneration of astrocyte and small dendritic processes. In the layers of pyramidal neurons (layers III and V of the SMC), significantly more terminals probably underwent the «lucid-type» destruction, with a determination coefficient of 72 and 80%, respectively. These differences in SMC layers could be due to the fact that the molecular layer contains significantly more fibrous astrocyte processes [26]. This probably allows efficient water reabsorption from edematous terminals, preventing their irreversible death through the lucid-type destruction mechanism. On the other hand, layer III of the SMC, which had maximal intensity neuropil edema and swelling and neuronal damage, showed the maximum decrease in the relative area of p38-positive material. Apparently, in this layer, the mechanisms of water reabsorption were disrupted which entailed the destruction of synaptic vesicles and terminals in general.

Our findings will help clarify the nature of reorganization of the components of different neuronal complexes of SMCs in relation to the possible de- and hyperhydration of neural tissue after LCCA.

## Conclusion

After bilateral irreversible LCCA, destruction, compensation and restoration were observed in neurons, glial cells, and inter-neuronal communication structures in layers I, III, and V of the rat SMC. Reorganization of neuroglial and inter-neuronal interrelations occurred with the underlying severe neuropil hyperhydration, perikaryon dehydration and reactive gliosis. These SMC changes appeared at different time points. Thus, the numerical density of microgliocytes reached its maximum values on day 1, oligodendrocytes on days 7 and 14, and astrocytes on day 14. Maximum destruction of neurons and synaptic terminals was observed in layer III of

SMC. Overall, all these changes resulted in a significant heterogeneity of the neural tissue response to LCCA. The secondary projection complex of the SMC was affected to a greater extent. This should be taken into account when studying the pathophysiology of changes in SMC structure.

Authors' participation: the authors personally and equally participated in the implementation of the comphrehensive approach including the experimental, anatomical, histological, morphometric and mathematical methods, as well as methods of observation, description and analysis.

## References


1. *Бонь Е.И., Максимович Н.Е., Валько Н.А.* Головной мозг крысы (обзор). Оренбургский медицинский вестник. 2022; 10 2 (38): 5–11. [*Bon E.I., Maksimovich N.E., Valko N.A.* Rat brain (review). *Orenburg Medical Bulletin/Orenburgsky Meditsinsky Vestnik*. 2022; 10 2 (38): 5–11. (in Russ.)].
2. *Зиматкин С.М., Маслакова С.М., Бонь Е.И.* Строение и развитие коры головного мозга крысы. Гродно. *ГрГМУ*. 2019: 156. [*Zimatkin, S.M., Maslakova S.M., Bon E.I.* Structure and development of the rat cerebral cortex. Grodno. *GrSMU*, 2019: 156. (in Russ.)].
3. *Зиматкин С.М.* Закономерности постнатального развития нейронов мозга. *Журнал Гродненского государственного медицинского университета*. 2021; 19 (1): 106–111. DOI: 10.25298/2221-8785-2021-19-1-106-111. [*Zimatkin S.M.* Patterns of postnatal development of brain neurons. *Journal of Grodno State Medical University/Zhurnal Grodnenskogo Meditsinskogo Universiteta*. 2021; 19 (1): 106–111. (in Russ.). DOI: 10.25298/2221-8785-2021-19-1-106-111].
4. *Обухов Д.К., Цехмистренко Т.А., Пущина Е.В., Вараксин А.А.* Формирование популяций нейронов и нейроглии в пре- и постнатальном развитии ЦНС позвоночных животных. *Морфология*. 2019; 156 (6): 57–63. [*Obukhov D.K., Tsekhmistrenko T.A., Pushchina E.V., Varaksin A.A.* Formation of populations of neurons and neuroglia in pre- and postnatal development of the central nervous system of vertebrates. *Morphology*. 2019; 156 (6): 57–63. (in Russ.)].
5. *Qian H-Z., Zhang H., Yin L-L., Zhang J-J.* Postischemic housing environment on cerebral metabolism and neuron apoptosis after focal cerebral ischemia in rats. *Curr Med Sci*. 2018; 38 (4): 656–665. DOI: 10.1007/s11596-018-1927-9. PMID: 30128875.
6. *Koizumi S., Hirayama Y., Morizawa Y. M.* New roles of reactive astrocytes in the brain; an organizer of cerebral ischemia. *Neurochem Int*. 2018; 119 (10): 107–114. DOI: 10.1016/j.neuint.2018.01.007. PMID: 29360494.
7. *Авдеев Д. Б., Акулинин В.А., Степанов С.С., Шоронова А.Ю., Макарьева Л.М., Горбунова А.В., Коржук М.С., Маркелова М.В.* Влияние окклюзии общих сонных артерий на двуядерные клеточные образования сенсомоторной коры большого мозга крыс. *Общая реаниматология*. 2021; 17 (2): 55–71. DOI: 10.15360/1813-9779-2021-2-55-71. [*Avdeev D.B., Akulinin V.A., Stepanov S.S., Shoronova A.Yu., Makarieva L.M., Gorbunova A.V., Korzhuk M.S., Markelova M.V.* The effect of occlusion of the common carotid arteries on the binucleated cell formations of the sensorimotor cortex of the rat brain. *General reanimatology/ Obshchaya reanimatologya*. 2021; 17 (2): 55–71. (in Russ.). DOI: 10.15360/1813-9779-2021-2-55-71].
8. *Макарьева Л.М, Акулинин В.А., Степанов С.С., Шоронова А.Ю., Авдеев Д.Б., Коржук М.С.* Морфологическое и морфометрическое описание нейронов сенсомоторной коры головного мозга крыс после перевязки общих сонных артерий. *Журнал анатомии и гистопатологии*. 2022; 11 (1); 49–58. DOI: 10.18499/2225-7357-2022-11-1-49-58. [*Makarieva L.M., Akulinin V.A., Stepanov S.S., Shoronova A.Yu., Avdeev D.B., Korzhuk M.S.* Morphological and morphometric description of neurons of the sensorimotor cortex of rats after ligation of common carotid arteries. *Journal of Anatomy and Histopathology/Zhurnal Anatomii i Gistopatologii*. 2022; 11 (1); 49–58. (in Russ.). DOI: 10.18499/2225-7357-2022-11-1-49-58].
9. *Макарьева Л.М., Коржук М.С., Акулинин В.А., Степанов С.С., Шоронова А.Ю., Авдеев Д.Б.* Нейроглиальные взаимоотношения и структуры межнейронной коммуникации слоя V сенсомоторной коры белых крыс после перевязки общих сонных артерий. *Журнал анатомии и гистопатологии*. 2022; 11 (2): 43–51. DOI: 10.18499/2225-7357-2022-11-2-43-51. [*Makarieva L.M., Korzhuk M.S., Akulinin V.A., Stepanov S.S., Shoronova A.Yu., Avdeev D.B.* Neuroglial relationships and structures of interneuronal communication of layer V of the sensorimotor cortex of white rats after ligation of the common carotid arteries. *Journal of Anatomy and Histopathology/Zhurnal Anatomii i Gistopatologii*. 2022; 11 (2): 43–51. (in Russ.). DOI: 10.18499/2225-7357-2022-11-2-43-51].
10. *Бонь Е. И., Максимович Е. И.* Сравнительный анализ морфологических нарушений нейронов теменной коры и гиппокампа крыс при различных видах экспериментальной ишемии головного мозга. *Оренбургский медицинский вестник*. 2021; 92 (34): 29–37. [*Bon E.I., Maksimovich E.I.* Comparative analysis of morphological disorders of neurons of the parietal cortex and hippocampus of rats in various types of experimental cerebral ischemia. *Orenburg Medical Bulletin/ Orenburgsky Meditsinsky Vestnik*. 2021; 92 (34): 29–37. (in Russ.)].
11. *Антоненко Л.М., Вахнина Н.В., Громова Д.О.* Когнитивные нарушения, головокружение и неустойчивость у пациентов с артериальной гипертензией. *Неврология, нейропсихиатрия, психосоматика*. 2020; 12 (5): 92–97. DOI 10.14412/2074-2711-2020-5-92–97. [*Antonenko L.M., Vakhnina N.V., Gromova D.O.* Cognitive disorders, dizziness and instability in patients with arterial hypertension. *Neurology, neuropsychiatry, psychosomatics/Nevrologiya Neiropsikhiatriya, Psikhosomatika*. 2020; 12 (5): 92–97. (in Russ.). DOI 10.14412/2074-2711-2020-5-92-97].
12. *Jing Z., Shi C., Zhu L., Xiang Y., Chen P, Xiong Z., Li W., Ruan Y., Huang L.* Chronic cerebral hypoperfusion induces vascular plasticity and hemodynamics but also neuronal degeneration and cognitive impairment. *J Cereb Blood Flow Metab*. 2015; 35 (8): 1249–1259. DOI: 10.1038/jcbfm.2015.55. PMID: 25853908.
13. *Paxinos G, Watson C.* The rat brain in stereotaxic coordinates. 5th ed. *Elsevier Academic Press*. Amsterdam, Boston. 2005. eBook ISBN: 9780080474120.
14. *Боровиков В.* Statistica. Искусство анализа данных на компьютере. 2-ое изд. СПб. Питер. 2003: 688. [*Borovikov V.* Statistica. The art of data analysis on a computer. 2nd ed. St. Petersburg: Piter; 2003: 688. (in Russ.)].

15. *Коржевский Д.Э., Кирик О.В., Сухорукова Е.Г., Власов Т.Д.* Структурная организация микроглиоцитов стриатума после транзиторной фокальной ишемии. *Морфология*. 2012; 141 (2): 28–32. [*Korzhevsky D.E., Kirik O.V., Sukhorukova E.G., Vlasov T.D.* Structural organization of striatum microglyocytes after transient focal ischemia. *Morphology/Morfologiya*. 2012; 141 (2): 28–32. (in Russ.)].
16. *Бонь Е.И., Максимович Н.Е., Малыхина А.В.* Нейроглия и ее роль в патогенезе ишемического повреждения головного мозга. Иммуногистохимические маркеры нейроглии. *Вестник Смоленской государственной медицинской академии*. 2021; 20 (3): 18–24. DOI: 10.37903/vsgma.2021.3.3. [*Bon E.I., Maksimovich N.E., Malykhina A.V.* Neuroglia and its role in the pathogenesis of ischemic brain damage. immunohistochemical markers of neuroglia. *Bulletin of the Smolensk State Medical Academy/Vestnik Smolenskoy Gosudarstvennoy Meditsinskoy Akademii*. 2021; 20 (3): 18–24. (in Russ.). DOI: 10.37903/vsgma.2021.3.3].
17. *Пальцын А.А., Свиридкина Н.Б.* О регенерации мозга (лекция II). *Патогенез*. 2018; 16 (1): 83–91. DOI: 10.25557/2310-0435.2018.01.83-91. [On brain regeneration (lecture two). *Pathogenesis/Patogenez*. 2018; 16 (1): 83–91. (in Russ.). DOI: 10.25557/2310-0435.2018.01.83-91].
18. *Кириченко Е.Ю., Логвинов А.К., Филиппова С.Ю., Арефьев Р.А., Семынина В.Г., Лысенко Л.В.* Особенности строения нейро-глио-сосудистых ансамблей в гломерулах обонятельной луковицы крысы. *Цитология*. 2020; 62 (4): 278–285. DOI: 10.31857/S0041377120040057 [*Kirichenko E.Yu., Logvinov A.K., Filippova S. Yu., Arefyev R.A., Semynina V.G., Lysenko L.V.* Structural features of neuro-glio-vascular ensembles in the glomeruli of the rat olfactory bulb. *Cytology/Tsytologiya*. 2020; 62 (4): 278–285. DOI: 10.31857/S0041377120040057. (in Russ.)].
19. *Arizono M., Krishna Inavalli V. V. G., Panatier A., Pfeiffer T., Angibaud J., Levet F., Ter Veer M. J.T., Stobart J., Bellocchio L., Mikoshiba K., Marsicano G., Weber B., Oliet S. H. R., Nägerl U. V.* Structural basis of astrocytic $Ca^{2+}$ signals at tripartite synapses. *Nat Commun*. 2020; 11 (1): 1906. DOI: 10.1038/s41467-020-15648-4. PMID: 32312988.
20. *Калинина Ю.А., Гилерович Е.Г., Коржевский Д.Э.* Астроциты и их участие в механизмах терапевтического действия мультипотентных мезенхимальных стромальных клеток при ишемическом повреждении головного мозга. *Гены и клетки*. 2019; 14 (1): 33–40. DOI: 10.23868/201903004. [*Kalinina Yu.A., Gilerovich E.G., Korzhevsky D.E.* Astrocytes and their participation in the mechanisms of therapeutic action of multipotent mesenchymal stromal cells in ischemic brain injury. *Genes and Cells/Geny i Kletki*. 2019; 14 (1): 33–40. (in Russ.). DOI: 10.23868/201903004].
21. *Степанов А.С., Акулинин В.А., Степанов С.С., Авдеев Д.Б.* Клеточные системы восстановления и утилизации поврежденных нейронов головного мозга белых крыс после 20-минутной окклюзии общих сонных артерий. *Российский физиологический журнал им. И.М. Сеченова*. 2017; 103 (10): 1135–1147. [*Stepanov A.S., Akulinin V.A., Stepanov S.S., Avdeev D.B.* Cellular systems of rehabilitation and utilization of damaged neurons of the brain of white rats after 20-minute occlusion of the common carotid arteries. *I.M. Sechenov Russian Journal of Physiology/ Ross. Fiziol. Zh. Im. I.M. Sechenova*. 2017; 103 (10): 1135–1147. (in Russ.)].
22. *Боголепова И.Н., Малофеева Л.И., Агапов П.А., Малофеева И.Г.* Изменения цитоархитектоники префронтальной коры мозга мужчин и женщин в зрелом и пожилом возрасте. *Журнал анатомии и гистопатологии*. 2017; 6 (3): 13–18. DOI: 10.18499/2225-7357-2017-6-3-13-18 [*Bogolepova I.N., Malofeeva L.I., Agapov P.A., Malofeeva I.G.* Cytoarchitecture changes in the of the prefrontal brain cortex of adult and aged men and women. *Journal of Anatomy and Histopathology/Zhurnal Anatomii i Gistopatologii*. 2017; 6 (3): 13–18. (in Russ.). DOI: 10.18499/2225-7357-2017-6-3-13-18].
23. *Ишунина Т.А., Боголепова И.Н., Свааб Д.Ф.* Морфофункциональные изменения и компенсаторные механизмы в головном мозге человека при старении и болезни Альцгеймера. *Журнал анатомии и гистопатологии*. 2020; 9 (1): 77–85. DOI: 10.18499/2225-7357-2020-9-1-77-85 [*Ishunina T.A., Bogolepova I.N., Svaab D.F.* Morphofunctional changes and compensatory mechanisms in the human brain with aging and in Alzheimer's disease. *Journal of Anatomy and Histopathology/ Zhurnal Anatomii i Gistopatologii*. 2020; 9 (1): 77–85. (in Russ.). DOI: 10.18499/2225-7357-2020-9-1-77-85].
24. *Isgrò M.A., Bottoni P., Scatena R.* Neuron-specific enolase as a biomarker: biochemical and clinical aspects. *Adv Exp Med Biol*. 2015; 867: 125–143. DOI: 10.1007/978-94-017-7215-0_9. PMID: 26530364.
25. *Li Q., Zhang R., Ge Y-l., Mei Y-w, Guo Y-l.* Effects of neuregulin on expression of MMP-9 and NSE in brain of ischemia/reperfusion rat. *J Mol Neurosci*. 2009; 38 (2): 207–215. DOI: 10.1007/s12031-008-9150-y. PMID: 18830828.
26. *Авдеев Д.Б., Степанов С.С., Акулинин В.А., Степанов А.С., Шоронова А.Ю., Самсонов А.А.* Реорганизация астроцитов гиппокампа белых крыс после 20-минутной окклюзии общих сонных артерий. *Патологическая физиология и экспериментальная терапия*. 2019; 63 (4): 13–22. DOI: 10.25557/0031-2991.2019.04.13-22. [*Avdeev D.B., Stepanov S.S., Akulinin V.A., Stepanov A.S., Shoronova A.Yu., Samsonov A.A.* Reorganization of hippocampal astrocytes of white rats after 20-minute occlusion of common carotid arteries. *Pathological Physiology and Experimental Therapy/ Patol.Fiziol. Exsp. Ter.* 2019; 63 (4): 13–22. (in Russ.). DOI: 10.25557/0031-2991.2019.04.13-22].

**Received 31.05.2022**
**Online First 03.10.2022**